1-1-2019

Taylor's slope stability chart for combined effects of horizontal and vertical seismic coefficients

Pragyan Sahoo
Edith Cowan University, p.sahoo@ecu.edu.au

Sanjay Kumar Shukla
Edith Cowan University, s.shukla@ecu.edu.au

Recommended Citation

Sahoo, P., & Shukla, S. K. (2019). Taylor's slope stability chart for combined effects of horizontal and vertical seismic coefficients. DOI: https://doi.org/10.1680/jgeot.17.p.222

10.1680/jgeot.17.p.222
Originally published as: Sahoo, P. P., & Shukla, S. K. (2019). Taylor's slope stability chart for combined effects of horizontal and vertical seismic coefficients. *Géotechnique, 69*(4), 344-354. Original article available here.

Sahoo, P. P. & Shukla, S. K. (2019). *Géotechnique* **69**, No. 4, 344–354 [https://doi.org/10.1680/jgeot.17.P.222]

Taylor's slope stability chart for combined effects of horizontal and vertical seismic coefficients

P. P. SAHOO* and S. K. SHUKLA†

Design standards and codes of practice on earth slope stability often recommend the pseudo-static method of analysis for determining the factor of safety of a slope subjected to seismic forces. In most pseudo-static methods of analysis, the horizontal seismic force is considered without due weightage to vertical seismic force. In the past, Taylor's stability chart for a homogeneous cohesive-frictional soil slope has been extended to consider the effect of horizontal seismic force only. In this paper, an attempt is made to develop an analytical formulation considering both horizontal and vertical seismic forces in order to estimate the factor of safety of the homogeneous, cohesive-frictional soil slopes with simple profiles using Taylor's stability chart. The analytical formulation is based on the friction circle method, which is one of the methods of static slope stability analysis. Several field cases have been analysed considering slope geometry, soil properties and seismic loading conditions so that Taylor's stability chart can be routinely used by practising engineers considering the effects of both horizontal and vertical seismic forces. An illustrative example is included in order to explain how practising engineers can use the graphical presentations developed in this paper as the design charts for stability analysis. This illustrative example has also been solved using Plaxis 2D, a commercially available finite-element software, as a comparison.

KEYWORDS: dynamics; earthquakes; failure; finite-element modelling; seismicity; slopes

INTRODUCTION

The stability of soil slope is always a great topic of debate for geotechnical engineers. In several routine applications, Taylor's stability chart (Taylor, 1937, 1948) is used as the main tool for the determination of the factor of safety F of finite homogeneous slopes consisting of c–ϕ soils under undrained conditions; c being the cohesion intercept and ϕ the angle of internal friction of soil under static conditions (e.g. Terzaghi *et al.*, 1996; Das, 2010; Shukla, 2015). Apart from Taylor's slope stability chart, several analytical methods have been developed in the past in order to have more realistic estimation of the factor of safety of slopes under static (Janbu, 1954; Bishop, 1955; Morgenstern & Price, 1965; Spencer, 1967) and dynamic/seismic (Majumdar, 1971; Sarma, 1973, 1979) conditions, considering different field situations and assumptions (Chowdhury *et al.*, 2010; Cheng & Lau, 2014; Duncan *et al.*, 2014). Under static loading condition, when the slope inclination and angle of internal friction of soil are known, then a stability number can be computed easily from Taylor's stability chart under static loading conditions. However, this design chart does not consider the estimation of factor of safety under the application of seismic force. It would be more advantageous to field engineers if Taylor's chart could further be used when both static and dynamic loading conditions exist, because stability of the slope becomes more critical under such circumstances. Majumdar (1971) explained how Taylor's stability chart can be used under the application of horizontal earthquake force by defining a modified friction angle of the c–ϕ soil, taking into account the horizontal seismic coefficient. Although most of the studies discuss the effect of horizontal earthquake force on stability of the slope, it has been found that the vertical component of earthquake force cannot be disregarded, as it greatly alters the effect of dynamic stress distribution (Chopra, 1966). Ling *et al.* (1997, 1999) and Shukha & Baker (2008) found that the vertical seismic force has significant effects on the stability of the slope. From past earthquake records, such as Loma Prieta (Lew, 1991), the Northridge earthquake (Stewart *et al.*, 1994) and the Hanshin earthquake (Bardet *et al.*, 1995), it has been found that the maximum vertical seismic force can be equal to or even greater than the horizontal seismic force. Aoi *et al.* (2008) reported that the vertical seismic acceleration was twice the horizontal seismic acceleration during the Iwate-Miyagi earthquake in Japan. Ling & Leshchinsky (1998) also reported that the vertical seismic acceleration was 30% larger than the horizontal seismic acceleration in the Hanshin earthquake. Ling *et al.* (1997) examined the stability and displacement of a slope under seismic action by using the log-spiral method and observed that, when the vertical acceleration was accompanied by horizontal acceleration, a prominent effect could be observed. Therefore, in this paper, an attempt is made to extend Majumdar's work (Majumdar, 1971) for the use of Taylor's stability chart under the combined actions of horizontal and vertical seismic forces. The developed approach will help practising engineers to analyse the stability of homogeneous slopes with simple profiles more realistically in earthquake-prone areas, using Taylor's stability chart in a simple way, without depending on the need for any commercial software or the development of an original numerical model.

Manuscript received 29 August 2017; revised manuscript accepted 18 May 2018. Published online ahead of print 18 June 2018.
Discussion on this paper closes on 1 September 2019, for further details see p. ii.

* Discipline of Civil and Environmental Engineering, School of Engineering, Edith Cowan University, Perth, WA, Australia (Orcid:0000-0002-6788-0415).
† Discipline of Civil and Environmental Engineering, School of Engineering, Edith Cowan University, Perth, WA, Australia (Orcid:0000-0002-4685-5560).

ANALYTICAL FORMULATION

Using the modified friction circle method, Taylor (1937, 1948) presented a slope stability chart, as shown in Fig. 1, which provides a relationship between the stability number $c/F\gamma H$ and slope angle i for different values of the angle of internal friction ϕ of the soil, with c, γ, H and F as the cohesion intercept, total unit weight of soil, height of slope and factor of safety of the slope, respectively. This chart is based on the following assumptions.

(*a*) The entire soil mass forming the slope is homogeneous.
(*b*) The potential failure surface passes through the toe of the slope and is cylindrical (Fig. 2).
(*c*) When the soil mass is on the verge of failure, the failure surface follows the limiting condition of equilibrium, and hence, the shearing strength of the soil s can be expressed in the form of the Mohr–Coulomb criterion as

$$s = c + \sigma \tan \phi \tag{1}$$

where σ is the total normal stress on the failure surface.
(*d*) The analysis is based on total stresses and assumes that the cohesion c is constant with depth.

Considering all these assumptions and following the approach explained by Majumdar (1971), a modified friction angle (ϕ_m) of the c–ϕ soil can be derived as explained below, for the generalised seismic conditions, so that Fig. 1 can also be used as the design chart for determining the factor of safety of the soil slope subjected to both horizontal and vertical seismic loads.

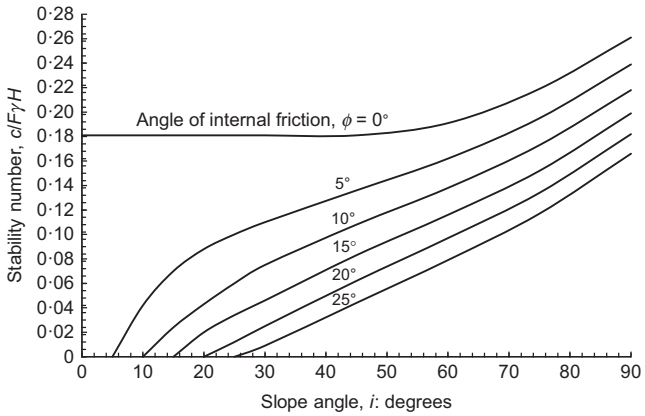

Fig. 1. Stability chart for c–ϕ soil slope (after Taylor, 1937, 1948)

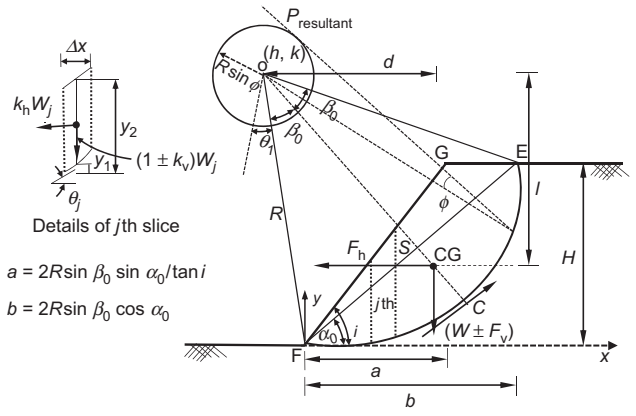

Fig. 2. Stability analysis due to the horizontal and vertical earthquake forces on the slope (adapted from Majumdar, 1971)

Figure 2 shows a soil slope of height H with inclination i to the horizontal with a soil mass tending to slide over a cylindrical failure surface with its cross-section FE as the circular arc having its radius R and centre at O (h, k). The position of the centre O (h, k) is defined by two angles, namely the central angle of the failure arc ($2\beta_0$) and the angle made by the chord EF with the horizontal of the slope (α_0). The forces acting on the sliding mass FGE are as follows (Fig. 2)

(*a*) weight, W, of the sliding mass, acting vertically downward at the centre of gravity (CG)
(*b*) horizontal seismic load, F_h acting outward, and vertical seismic load, F_v acting either in upward (↑) or downward (↓) directions on the sliding mass at the centre of gravity
(*c*) the total resultant cohesion C of the slope along the failure arc
(*d*) the resultant ($P_{resultant}$) of normal force and frictional force intersecting with the line of action of W, which makes an angle ϕ with the normal to the failure circle. As a result, the line of action of the resultant force will remain tangent to the circle of radius $R\sin\phi$, also known as the friction circle shown in the figure.

It is assumed that if the weight W_E of the sliding mass, including both horizontal and vertical seismic loads, F_h and F_v, is expressed in terms of an equivalent total unit weight γ_E; then the total overturning moment due to the weight W of the potential sliding mass and combined seismic loads, F_h and F_v, will give the same overturning moment as produced by the equivalent weight W_E. As γ_E is the equivalent total unit weight, this gives

$$W_E = \gamma_E V \tag{2}$$

where V is the volume of the potential sliding soil mass. It may be noted that the weight W is given by

$$W = \gamma V \tag{3}$$

where γ is the total unit weight of soil of the slope.

Horizontal seismic/earthquake force

$$F_h = k_h W \tag{4}$$

where k_h is the pseudo-static horizontal seismic coefficient.

Vertical seismic/earthquake force

$$F_v = \pm k_v W \tag{5}$$

where k_v is the pseudo-static vertical seismic coefficient. It may be noted that, in equation (5), the positive (+) sign indicates that F_v acts in the vertically downward direction (↓), whereas the negative (−) sign indicates that F_v acts in the vertically upward direction (↑).

Taking the moment of forces about the centre of the circle O

$$W_E d = (W \pm F_v)d + F_h l \tag{6}$$

where l is the moment arm of the force F_h and d is the moment arm of the force F_v and W.

Using equations (2)–(5), equation (6) becomes

$$\gamma_E V d = (\gamma V \pm k_v \gamma V)d + k_h \gamma V l$$

or

$$\gamma_E = \gamma\left(1 \pm k_v + k_h \frac{l}{d}\right) \tag{7}$$

Considering a vertical jth slice of the sliding soil mass of unit thickness with weight W_j, width Δx and slice side lengths y_2 and y_1, as shown in Fig. 2, and subjected to both horizontal seismic force F_h and vertical seismic force F_v, the total resisting force S besides cohesion (assumed to be independent of seismic/dynamic conditions) can be expressed as follows

$$S = \sum_{x=0}^{x=b} \left[(1 \pm k_v) W_j \cos\theta_j - W_j k_h \sin\theta_j\right] \tan\phi$$

or

$$S = \gamma \sum_{x=0}^{x=b} \left[(1 \pm k_v)(y_2 - y_1)\cos\theta_j - k_h (y_2 - y_1)\sin\theta_j\right] \Delta x \tan\phi \tag{8}$$

where θ_j is the angle made by the base of the jth slice with the horizontal and b denotes the limit of the area bounded by the sliding mass, as shown in the figure, and is expressed as follows

$$b = 2R \sin\beta_0 \cos\alpha_0 \tag{9}$$

The total effect due to combined seismic load can be represented in the form of total equivalent unit weight γ_E and modified friction angle ϕ_m. In this case, the resisting force is

$$S = \gamma_E \sum_{x=0}^{x=b} (y_2 - y_1)\cos\theta_j \Delta x \tan\phi_m \tag{10}$$

From equations (8) and (10), one has

$$\gamma \sum_{x=0}^{x=b} \left[(1 \pm k_v)(y_2 - y_1)\cos\theta_j - k_h (y_2 - y_1)\sin\theta_j\right] \Delta x \tan\phi = \gamma_E \sum_{x=0}^{x=b} (y_2 - y_1)\cos\theta_j \Delta x \tan\phi_m$$

or

$$m = \frac{\tan\phi_m}{\tan\phi} = \frac{\gamma}{\gamma_E}\left[1 \pm k_v - k_h \frac{\sum_{x=0}^{x=b}(y_2 - y_1)\sin\theta_j \Delta x}{\sum_{x=0}^{x=b}(y_2 - y_1)\cos\theta_j \Delta x}\right] \tag{11}$$

where m is the ratio of tangent of modified angle of internal friction of soil to the tangent of angle of internal friction of soil, and it may be termed the friction reduction factor. It may be noted that m ranges from 0 to 1.

Substituting the value of γ_E from equation (7) into equation (11)

$$m = \frac{\tan\phi_m}{\tan\phi} = \frac{1}{[1 \pm k_v + k_h(l/d)]} \times \left[1 \pm k_v - k_h \frac{\sum_{x=0}^{x=b}(y_2 - y_1)\sin\theta_j \Delta x}{\sum_{x=0}^{x=b}(y_2 - y_1)\cos\theta_j \Delta x}\right] \tag{12}$$

or

$$m = \frac{\tan\phi_m}{\tan\phi} = \frac{1}{[1 \pm k_v + k_h(l/d)]}\left(1 \pm k_v - k_h \frac{P}{Q}\right) \tag{13}$$

where

$$P = \sum_{x=0}^{x=b} (y_2 - y_1)\sin\theta_j \Delta x \tag{14a}$$

and

$$Q = \sum_{x=0}^{x=b} (y_2 - y_1)\cos\theta_j \Delta x \tag{14b}$$

For $k_v = 0$, equation (12) or (13) reduces to the case of consideration of only horizontal seismic force as Majumdar (1971) has considered. In his work, no attempt was made to present the simplified form of summation terms. So, in the following paragraph, an attempt is made in this direction, for which the integration concept has been used in place of summation for simplicity.

Equations (14a) and (14b) can be presented considering $\Delta x \to 0$ as

$$P = \int_{x=0}^{x=b} (y_2 - y_1)\sin\theta_j \mathrm{d}x$$

or

$$P = \int_{x=0}^{x=a} (y_2 - y_1)\sin\theta_j \mathrm{d}x + \int_{x=a}^{x=b} (y_2 - y_1)\sin\theta_j \mathrm{d}x \tag{15a}$$

and

$$Q = \int_{x=0}^{x=b} (y_2 - y_1)\cos\theta_j \mathrm{d}x$$

or

$$Q = \int_{x=0}^{x=a} (y_2 - y_1)\cos\theta_j \mathrm{d}x + \int_{x=a}^{x=b} (y_2 - y_1)\cos\theta_j \mathrm{d}x \tag{15b}$$

where

$$a = 2R \sin\beta_0 \sin\alpha_0 / \tan i \tag{16}$$

In Fig. 2, it is noticed that the potential sliding mass is bounded by line FG, line GE and circular arc FE (y_1) having centre at O (h, k). The equation of the line FG (y_2) can be defined as a function of x as

$$y_2 = x \tan i \tag{17}$$

As line GE is parallel to the x-axis

$$\mathrm{GE} = 2R \sin\beta_0 \sin\alpha_0 \tag{18}$$

The equation of the circle with centre O can be defined as

$$(x - h)^2 + (y_1 - k)^2 = R^2 \tag{19}$$

where h and k are the x and y coordinates of the centre O with their values as

$$h = R\sin(\beta_0 - \alpha_0) \tag{20a}$$

$$k = R\cos(\beta_0 - \alpha_0) \tag{20b}$$

Differentiating equation (19), the slope of the line can be obtained as

$$\tan\theta = \frac{\mathrm{d}y_1}{\mathrm{d}x} = -\frac{(x - h)}{(y_1 - k)}$$

Therefore

$$\sin\theta = \frac{x - h}{R} \tag{21a}$$

and

$$\cos\theta = -\frac{y_1 - k}{R} = -\frac{\sqrt{R^2 - (x-h)}}{R} \tag{21b}$$

Using equations (9) and (16)–(21b), equations (15a) and (15b) are expressed as

$$\begin{aligned}
P &= \int_0^{2R\sin\beta_0\sin\alpha_0/\tan i} (y_2 - y_1)\sin\theta_j + \int_{2R\sin\beta_0\sin\alpha_0/\tan i}^{2R\sin\beta_0\cos\alpha_0} (y_2 - y_1)\sin\theta_j \\
&= \int_0^{2R\sin\beta_0\sin\alpha_0/\tan i} \left\{ x\tan i - \left[k - \sqrt{R^2 - (x-h)^2} \right] \right\} \frac{x-h}{R}\,\mathrm{d}x \\
&\quad + \int_{2R\sin\beta_0\sin\alpha_0/\tan i}^{2R\sin\beta_0\cos\alpha_0} \left\{ 2R\sin\beta_0\sin\alpha_0 - \left[k - \sqrt{R^2 - (x-h)^2} \right] \right\} \frac{x-h}{R}\,\mathrm{d}x \\
&= \frac{\tan i}{R}\left[\frac{x^3}{3} - h\frac{x^2}{2} \right]\Bigg|_0^{2R\sin\beta_0\sin\alpha_0/\tan i} - \frac{k}{R}\left[\frac{(x-h)^2}{2} \right]\Bigg|_0^{2R\sin\beta_0\sin\alpha_0/\tan i} \\
&\quad + \frac{1}{R}\left\{ -\frac{1}{3}\left[R^2 - (x-h)^2 \right]^{3/2} \right\}\Bigg|_0^{2R\sin\beta_0\sin\alpha_0/\tan i} \\
&\quad + \left(\frac{2R\sin\beta_0\sin\alpha_0 - k}{R} \right) \frac{(x-h)^2}{2}\Bigg|_{2R\sin\beta_0\sin\alpha_0/\tan i}^{2R\sin\beta_0\cos\alpha_0} \\
&\quad + \frac{1}{R}\left\{ -\frac{1}{3}\left[R^2 - (x-h)^2 \right]^{3/2} \right\}\Bigg|_{2R\sin\beta_0\sin\alpha_0/\tan i}^{2R\sin\beta_0\cos\alpha_0}
\end{aligned} \tag{22a}$$

and

$$\begin{aligned}
Q &= \int_0^{2R\sin\beta_0\sin\alpha_0/\tan i} (y_2 - y_1)\cos\theta_j\mathrm{d}x + \int_{2R\sin\beta_0\sin\alpha_0/\tan i}^{2R\sin\beta_0\cos\alpha_0} (y_2 - y_1)\cos\theta_j\mathrm{d}x \\
&= \int_0^{2R\sin\beta_0\sin\alpha_0/\tan i} \left\{ x\tan i - \left[k - \sqrt{R^2 - (x-h)^2} \right] \right\} \frac{\sqrt{R^2 - (x-h)^2}}{R}\,\mathrm{d}x \\
&\quad + \int_{2R\sin\beta_0\sin\alpha_0/\tan i}^{2R\sin\beta_0\cos\alpha_0} \left\{ 2R\sin\beta_0\sin\alpha_0 - \left[k - \sqrt{R^2 - (x-h)^2} \right] \right\} \frac{\sqrt{R^2 - (x-h)^2}}{R}\,\mathrm{d}x \\
&= \frac{\tan i}{R}\left\{ -\frac{1}{3}\left[R^2 - (x-h)^2 \right]^{3/2} \right\}\Bigg|_0^{2R\sin\beta_0\sin\alpha_0/\tan i} \\
&\quad + \frac{(h-k)\tan i}{R} + \frac{1}{2}\left[(x-h)\sqrt{R^2 - (x-h)^2} + R^2\sin^{-1}\left(\frac{x-h}{R} \right) \right]_0^{2R\sin\beta_0\sin\alpha_0/\tan i} \\
&\quad + \frac{1}{R}\left[R^2 x - \frac{(x-h)^3}{R} \right]\Bigg|_0^{2R\sin\beta_0\sin\alpha_0/\tan i} \\
&\quad + \frac{2R\sin\beta_0\sin\alpha_0 - R\cos(\beta_0 - \alpha_0)}{R}\frac{1}{2}\left[(x-h)\sqrt{R^2 - (x-h)^2} + R^2\sin^{-1}\left(\frac{x-h}{R} \right) \right]_{2R\sin\beta_0\sin\alpha_0/\tan i}^{2R\sin\beta_0\cos\alpha_0} \\
&\quad + \frac{1}{R}\left[R^2 x - \frac{(x-h)^3}{R} \right]\Bigg|_{2R\sin\beta_0\sin\alpha_0/\tan i}^{2R\sin\beta_0\cos\alpha_0}
\end{aligned} \tag{22b}$$

To calculate m from equation (12), it is essential to compute the moment arm ratio (l/d) for the given sliding soil mass. This can be done by considering the slope geometry as shown in Fig. 2. If $\bar{Y}$ is the distance from the centre O to the centre of gravity CG of the circular segment, then the expression for $\bar{Y}$ is derived as

$$\bar{Y} = \frac{2}{3} D \left[\frac{(R/D)^3 \cos\theta_1 - \cot\theta_1}{(R/D)^2(\pi/2 - \theta_1) - \cot\theta_1} \right] \quad (23)$$

where D is the perpendicular distance from centre O to the chord EF of the slope, and θ_1 is the subtended angle of the circular segment. The value θ_1 depends upon the inclination angle of the slope, and can be determined from the geometry of the slope in Fig. 2. The moment arm d of F_v and W can be estimated by considering the circular segment (area A_1) and the triangular segment (area A_2) as given by the following expression (Arredi, 1966)

$$d = \frac{a_1 A_1 + a_2 A_2}{A_1 + A_2} \quad (24)$$

where a_1 and a_2 represent the moment arms from the centre of the circle to the centre of gravity of the areas A_1 and A_2, respectively, which are expressed as follows

$$a_1 = \frac{H^3}{12}\left(\frac{1}{A_1}\right)\left(\frac{1}{\sin^2\alpha_0}\right) \quad (25a)$$

$$a_2 = \frac{H}{3}\left(\frac{3}{2\tan\beta_0}\right) - \frac{H}{3}\left(\frac{1}{2\tan\alpha_0}\right) + \frac{H}{3}\left(\frac{1}{\tan i}\right) \quad (25b)$$

$$A_1 = \frac{H^2}{4}\left(\frac{\beta_0 - \sin\beta_0\cos\beta_0}{\sin^2\beta_0\cos^2\beta}\right) \quad (25c)$$

$$A_2 = \frac{H^2}{2}\left(\frac{1}{\tan\alpha_0} - \frac{1}{\tan i}\right) \quad (25d)$$

Substituting values from equations (25a)–(25d) into equation (24), d is estimated, and using equations (23) and (24), the moment arm l is calculated for a given angle of inclination (i) and height of the slope (H). All the calculations are made in the spreadsheet for a set of slope angles as Taylor (1937) considered when developing his chart.

By substituting the values of P and Q from equations (22a) and (22b) into equation (12), m is calculated for any failure surface within the given soil slope. With known value of m for the specific case, ϕ_m is determined using the angle of internal friction of soil ϕ. For use of Taylor's stability chart (Fig. 1) to determine the factor of safety of the slope under effect of horizontal and vertical seismic loads, ϕ_m is used in place of ϕ.

The design value of the seismic coefficients can be determined by referring to the earthquake design manuals or standards as applicable at a particular location. The U.S. Army Corps of Engineers (USACE, 1989) recommends $k_v = 0{\cdot}5k_h$, while IS 1983 (Part 1) (BIS, 2002) recommends $k_v = (2/3)k_h$. In the present work, $k_v = 0{\cdot}5k_h$ has been considered.

RESULTS AND DISCUSSION

In the present study, the use of Taylor's chart can be made under the effect of combined seismic action by evaluating the modified friction angle of the soil from equation (11) and thus the factor of safety for a given soil slope can be determined. For this purpose, the height of the slope has been considered as 50 m only in order to observe the effect of combined seismic pseudo-static coefficients; although Majumdar (1971) considered about 40 different cases to analyse the effect of horizontal earthquake force for two different heights (50 ft (15·24 m) and 75 ft (22·86 m)). However, for different heights, the plot of dimensionless quantity l/d ratio in equation (12) against i with respect to different angles of internal friction of soil is found to be the same.

Figure 3 shows the variation of the moment arm ratio l/d with slope inclination i for different angles of internal friction of the soil. It is noticed that l/d does not depend on the seismic coefficients, as Majumdar (1971) also reported.

Figure 4 shows the variation of the friction reduction factor m with the horizontal seismic coefficient k_h for vertical seismic coefficient, $k_v = 0$, the slope angle $i = 30°$, and internal friction angle of the soil, $\phi = 5$–$25°$. It is observed that for any value of ϕ, m decreases non-linearly with an increase in k_h, the rate of decrease in m being significantly higher for lower values of k_h. For example, for $\phi = 5°$, as k_h increases from 0 to 0·1, m decreases by 0·24, whereas the decrease in m is 0·06 for an increase in k_h from 0·4 to 0·5. It should be noted that the m does not vary significantly with an increase in ϕ from 10° to 25°, and this variation has also been observed by Majumdar (1971).

Figures 5, 6, 7 and 8 show the variation of m with k_h as the design charts for the slope angles $i = 30°$, 45°, 60° and 75°, respectively, with $\phi = 5°$, 10°, 15°, 20°, 25° and $k_v = 0{\cdot}5k_h$. In these design charts, both vertically upward and downward directions for k_v have been considered. In all these design plots, it may be noted that for any slope angle, as k_h increases, the value of m decreases, resulting in a lower value of ϕ_m compared to soil friction angle ϕ as evident from the relationship in equation (12). Also, it is observed that for any value of k_h, the value of m is smaller when k_v acts vertically upward compared with the values when $k_v = 0$ or k_v is downward. For example, in Fig. 8(a), for $k_h = 0{\cdot}4$, the value of m is found to be 0·38 when k_v is upward but 0·52 with k_v downward. The value of m is further noted to be 0·46 in the absence of the vertical seismic coefficient. Thus, the variation of m depends upon the values of k_h and k_v as well as the direction of k_v. It is also noted from Figs 7(c)–7(e) and 8 that, with increase of k_h, m tends to zero for k_v being upward or

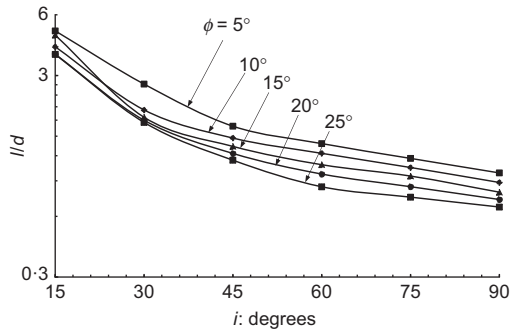

Fig. 3. Variation of moment arm ratio l/d with slope angle i for different angles of internal friction ϕ of soil

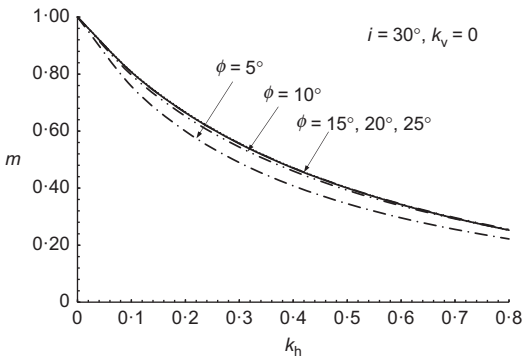

Fig. 4. Variation of friction reduction factor m with horizontal seismic coefficient k_h for different angles of internal friction of soil for slope angle $i = 30°$ and $k_v = 0$

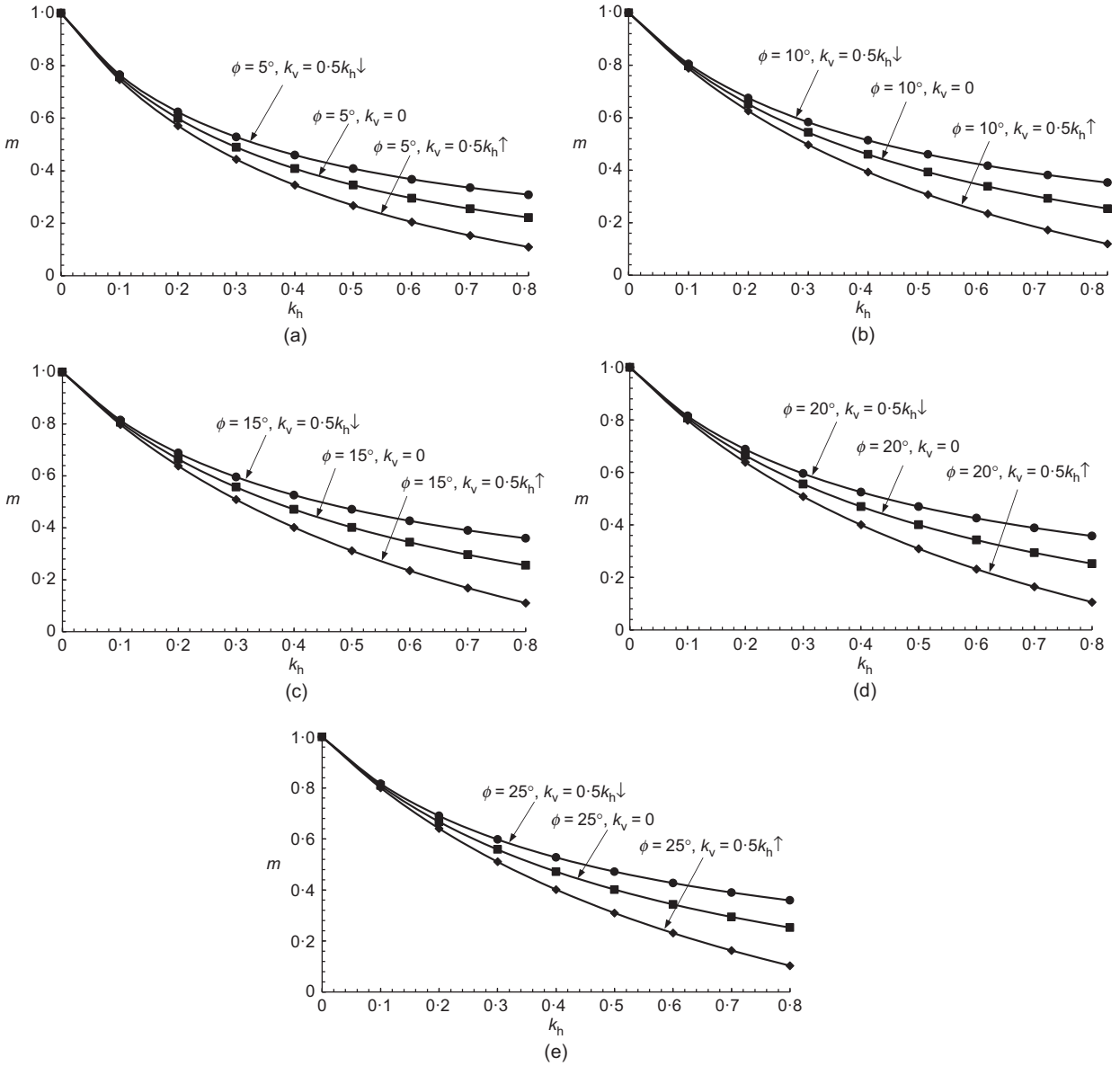

Fig. 5. Variation of reduction friction factor m with horizontal seismic coefficient k_h and vertical seismic coefficient k_v for: (a) $i = 30°$ and $\phi = 5°$; (b) $i = 30°$ and $\phi = 10°$; (c) $i = 30°$ and $\phi = 15°$; (d) $i = 30°$ and $\phi = 20°$; (e) $i = 30°$ and $\phi = 25°$

$k_v = 0$, which means that the friction angle as well as the modified friction angle of the soil under seismic conditions is zero. This suggests that soil may behave as an undrained case under earthquake conditions. This aspect can be used in Taylor's chart for the undrained case of c–ϕ soil slope under combined earthquake conditions.

ILLUSTRATIVE EXAMPLE

Consider a 10 m high soil slope with an inclination of 60° to the horizontal (Fig. 9). The soil has the following properties

total unit weight, $\gamma = 16$ kN/m^3
cohesion, $c = 20$ kPa
angle of internal friction, $\phi = 25°$

Determine the factor of safety under seismic conditions considering both horizontal and vertical seismic coefficients, for their following values

(*a*) $k_h = 0{\cdot}1$
(*b*) $k_h = 0{\cdot}5$

Assume $k_v = 0{\cdot}5k_h$.

Solutions

Solution to (*a*), with $k_h = 0{\cdot}1$, $k_v = 0{\cdot}5k_h = 0{\cdot}05$. From Fig. 7(e)

$$m \approx 0{\cdot}788$$

for both the vertically downward and upward directions of k_v.

From equation (11)

$$m = \frac{\tan\phi_m}{\tan\phi} = 0{\cdot}788$$

or

$$\phi_m = \tan^{-1}[0{\cdot}788(\tan\phi)]$$
$$= \tan^{-1}[0{\cdot}788(\tan 25°)]$$
$$= \tan^{-1}(0{\cdot}367)$$

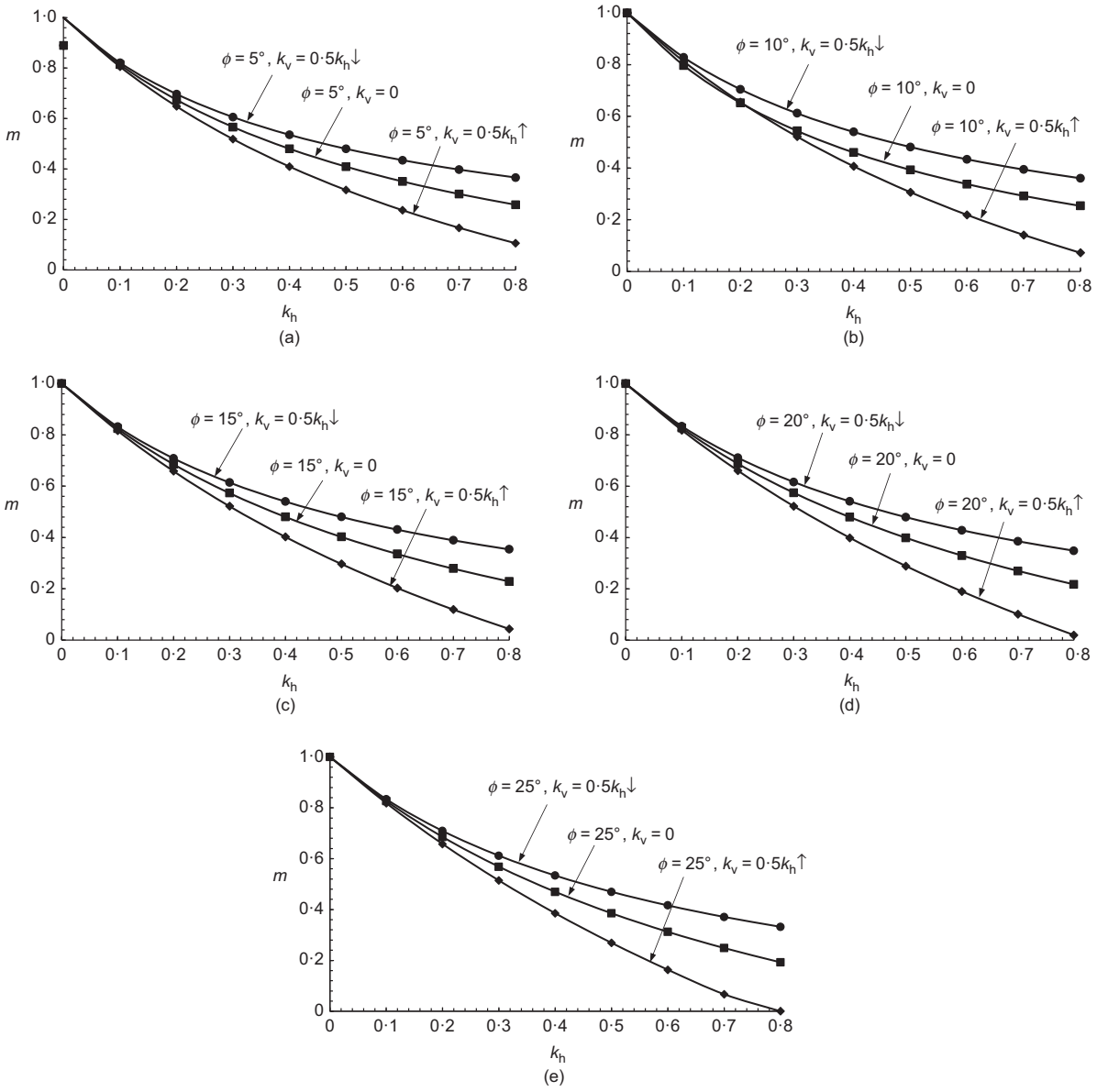

Fig. 6. Variation of reduction friction factor m with horizontal seismic coefficient k_h and vertical seismic coefficient k_v for: (a) $i = 45°$ and $\phi = 5°$; (b) $i = 45°$ and $\phi = 10°$; (c) $i = 45°$ and $\phi = 15°$; (d) $i = 45°$ and $\phi = 20°$; (e) $i = 45°$ and $\phi = 25°$

or

$$\phi_m \approx 20°$$

From Taylor's chart (Fig. 1), for slope angle, $i = 60°$ and $\phi_m = 20°$

$$\frac{c}{F\gamma H} = 0{\cdot}114$$

or

$$F = \frac{c}{(0{\cdot}114)\gamma H} = \frac{20}{(0{\cdot}114)(16)(10)} = 1{\cdot}09$$

Thus, the slope is apparently stable.

Solution to (*b*), with $k_h = 0{\cdot}5$, $k_v = 0{\cdot}5k_h = 0{\cdot}25$. From Fig. 7(e)

$$m \approx 0{\cdot}281$$

for vertically downward direction of k_v.

From equation (11)

$$m = \frac{\tan\phi_m}{\tan\phi} = 0{\cdot}281$$

or

$$\begin{aligned}\phi_m &= \tan^{-1}[0{\cdot}281(\tan\phi)] \\ &= \tan^{-1}[0{\cdot}281(\tan 25°)] \\ &= \tan^{-1}(0{\cdot}131)\end{aligned}$$

or

$$\phi_m \approx 7{\cdot}5°$$

From Taylor's chart (Fig. 1), for slope angle, $i = 60°$ and $\phi_m = 7{\cdot}5°$

$$\frac{c}{F\gamma H} = 0{\cdot}148$$

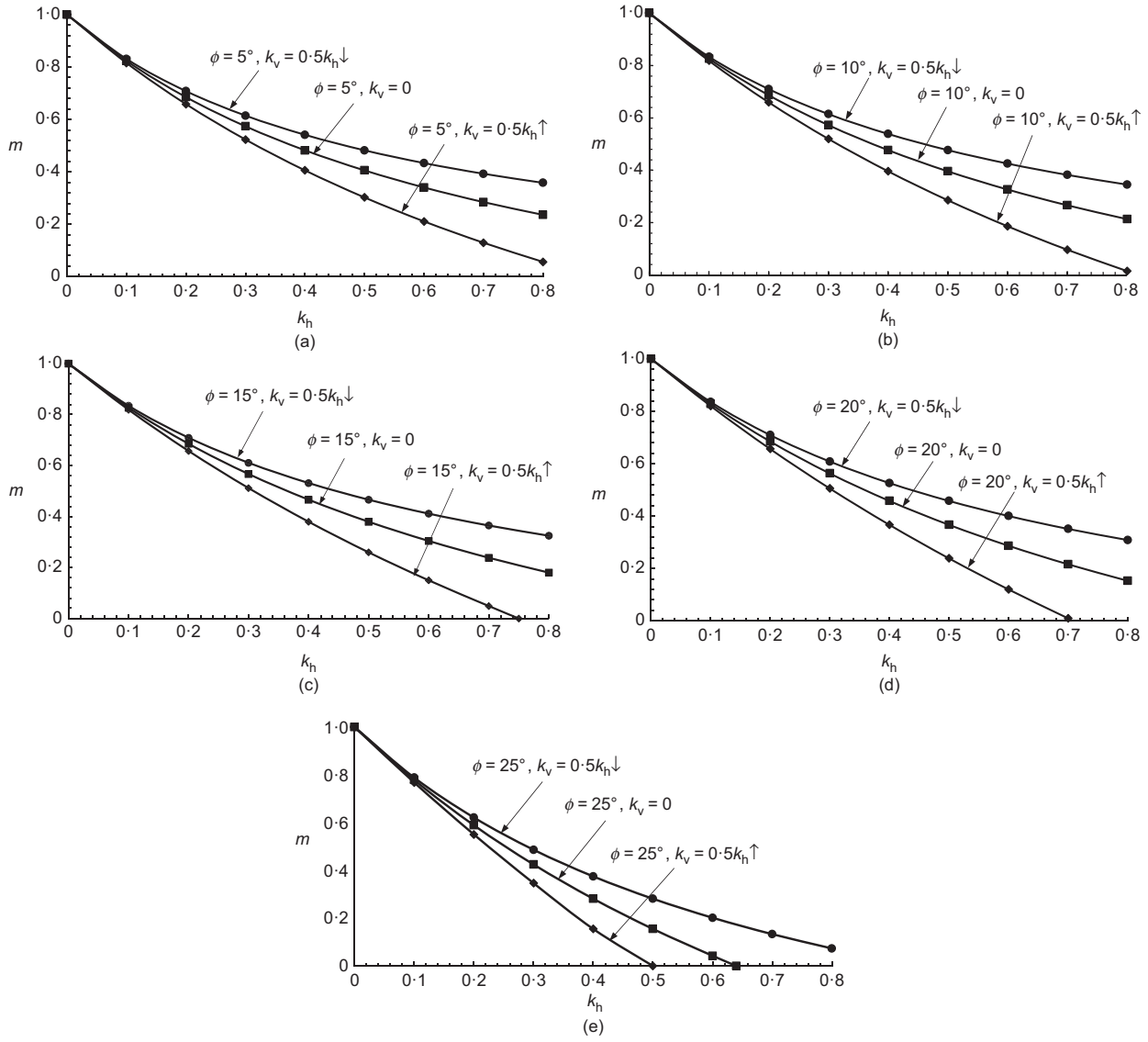

Fig. 7. Variation of reduction friction factor m with horizontal seismic coefficient k_h and vertical seismic coefficient k_v for: (a) $i = 60°$ and $\phi = 5°$; (b) $i = 60°$ and $\phi = 10°$; (c) $i = 60°$ and $\phi = 15°$; (d) $i = 60°$ and $\phi = 20°$; (e) $i = 60°$ and $\phi = 25°$

or

$$F = \frac{c}{(0{\cdot}148)\gamma H} = \frac{20}{(0{\cdot}148)(16)(10)} = 0{\cdot}844$$

Similarly, from Fig. 7(e)

$$m \approx 0$$

for vertically upward direction of k_v.

From equation (11)

$$m = \frac{\tan\phi_m}{\tan\phi} = 0$$

or

$$\phi_m = \tan^{-1}[0(\tan\phi)]$$
$$= \tan^{-1}[0(\tan 25°)]$$
$$= \tan^{-1}(0)$$

or

$$\phi_m = 0°$$

From Taylor's chart (Fig. 1), for slope angle, $i = 60°$ and $\phi_m = 0°$

$$\frac{c}{F\gamma H} = 0{\cdot}18$$

or

$$F = \frac{c}{(0{\cdot}18)\gamma H} = \frac{20}{(0{\cdot}18)(16)(10)} = 0{\cdot}694$$

For the comparison point of view, the stability of slopes considered in the illustrative example has been analysed by finite-element modelling using Plaxis 2D, which is a well-accepted commercially available software. The details are presented below.

Finite-element model and analysis

A two-dimensional (2D) plane-strain analysis with elastic–perfectly plastic Mohr–Coulomb soil criterion was used to model the slope considered in the illustrative example. Fifteen-noded triangular elements with 12 Gaussian points were used for the gravity load generation, the stiffness matrix generation and stress redistribution in order to simulate the

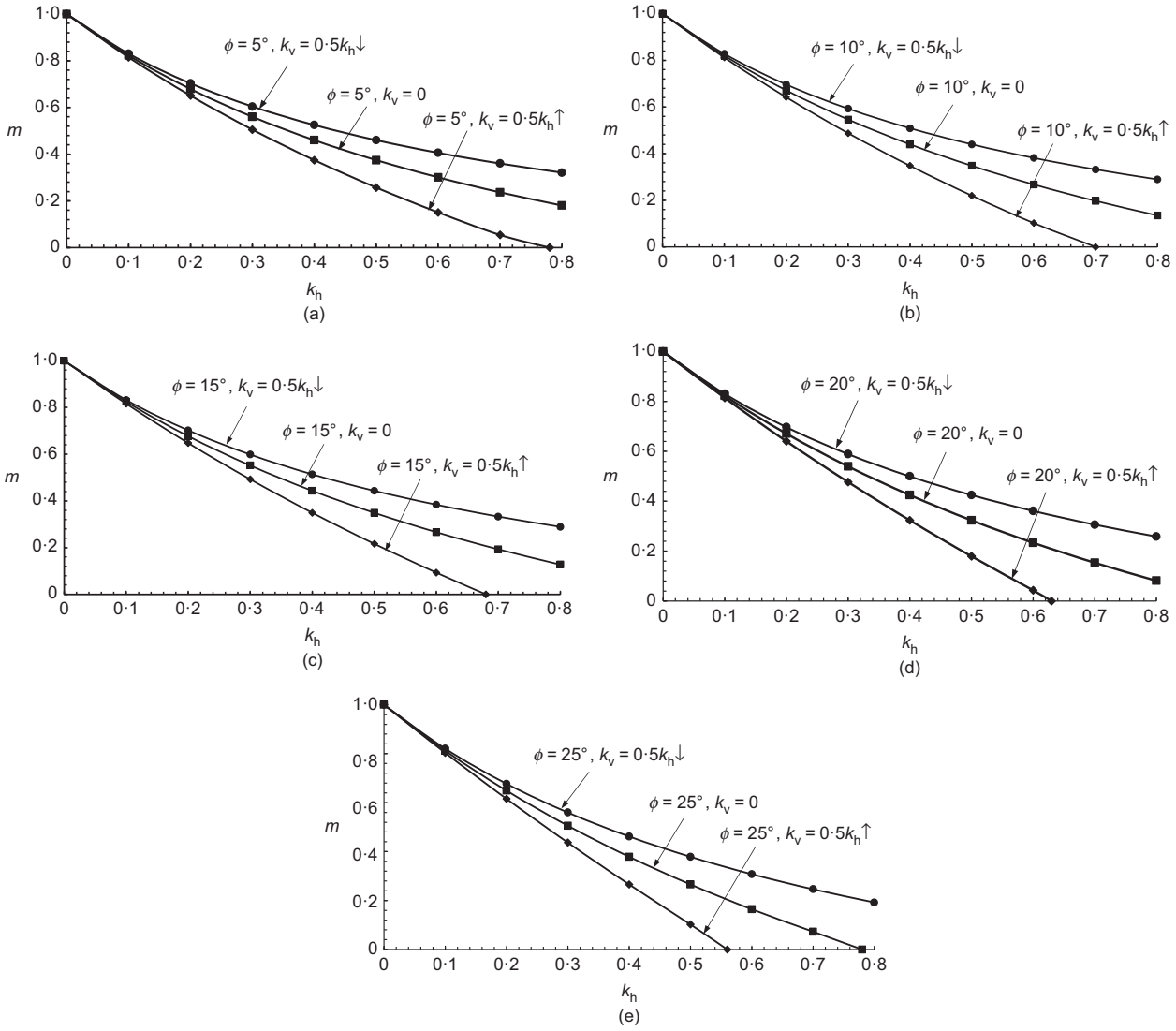

Fig. 8. Variation of reduction friction factor m with horizontal seismic coefficient k_h and vertical seismic coefficient k_v for: (a) $i = 75°$ and $\phi = 5°$; (b) $i = 75°$ and $\phi = 10°$; (c) $i = 75°$ and $\phi = 15°$; (d) $i = 75°$ and $\phi = 20°$; (e) $i = 75°$ and $\phi = 25°$

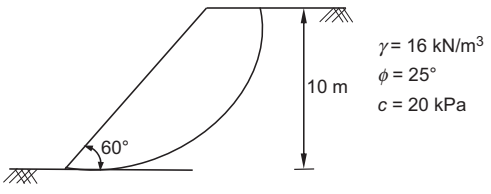

Fig. 9. Illustrative example for a homogeneous c–ϕ soil slope

accurate behaviour of soil slope under dynamic loading conditions (Al-Defae *et al*., 2013). Boundary conditions for the model were selected in such a manner so as to minimise the influence of stress distribution. In order to simulate a semi-infinite soil condition, full fixity was allowed to the base of the slope, while vertical boundaries were restrained in the horizontal direction. The soil model in Plaxis consists of six soil parameters, namely, effective shear strength parameters c' and ϕ', dilation angle ψ, total unit weight γ and elastic parameters as Young's modulus E' and Poisson ratio v'. The elastic parameters of soil have very little influence in the computation of factor of safety of the slope when compared to the deformation characteristic of soil. Therefore, in the absence of meaningful data, nominal values $E' = 10^5$ kN/m^2 and $v' = 0{\cdot}3$ were considered in the simulation process (Griffiths & Lane, 1999). As the stability analysis of slopes is relatively unconfined and the main objective of the current research is to predict the factor of safety, the dilation angle ψ was taken as zero considering no volume change during yielding of soil. It has been observed that the parameters of the finite-element soil model are the same as the parameters used in the traditional approach of the limit equilibrium method, namely, total unit weight γ and total shear strength parameters c and ϕ for a given geometry of the problem definition (Griffiths & Lane, 1999; Duncan *et al*., 2014). However, in the soil model, a foundation of depth 3 m was included to check whether the slip surface passes beyond the toe of the slope, and slope soil properties have been assigned to the foundation soil. Once the geometry was ready, the finite-element mesh was generated using the default medium-size mesh. The mesh should be fine enough to obtain accurate numerical results. Nevertheless, very fine meshing needs to be avoided considering its excessive calculation time (Plaxis, 2016). Fig. 10 shows the generated mesh of the soil slope. In order to evaluate the factor of safety of the soil slope considering pseudo-static conditions, the following two cases were considered in the numerical modelling

(*a*) gravity loading
(*b*) safety analysis.

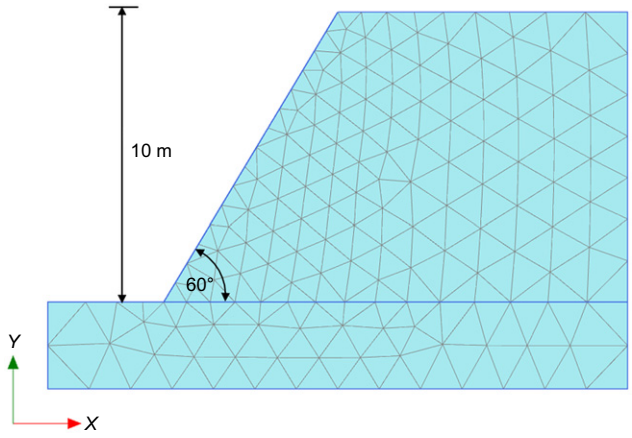

Fig. 10. Illustrative example: 2D numerical mesh for homogeneous c–ϕ soil slope

The initial state of stress of the slope was evaluated by considering the gravity-loading option in the preliminary phase of the modelling, where the forces of each element of mesh due to gravity were assembled into a global gravity force vector. The factor of safety of the slope was then calculated by using the principle of strength reduction method (Matsui & San, 1992), where the original strength parameters are divided by a factor to bring the sliding mass of the slope to the point of failure. It should be noted that, for computing the factor of safety using the pseudo-static option, it is essential to include the modal acceleration in the gravity-loading option. This is because Plaxis does not allow the user to include pseudo-static acceleration in the safety phase analysis.

Figure 11 shows the deformed shape of the slope under effect of combined seismic action with the seismic coefficient $k_h = 0{\cdot}1$ and $k_v = 0{\cdot}05(\downarrow)$. In the analysis, the iteration numbers were set to 60 for the convergence of the factor of safety. It has been observed that the factor of safety obtained for $k_h = 0{\cdot}1$ is 1·084, which is in good agreement with the analytical result having a factor of safety of 1·09, as mentioned in case (a) of the illustrative example with vertically downward direction of application of vertical seismic coefficient k_v. Although a factor of safety of 1·034 was evaluated for the vertically upward direction of seismic coefficient $k_v = 0{\cdot}05(\uparrow)$, for $\phi = 20°$ and $k_v = 0{\cdot}25(\uparrow\downarrow)$ of case (b) of the illustrative example, the slope collapses and Plaxis is unable to deliver the result if the factor of safety is less than unity.

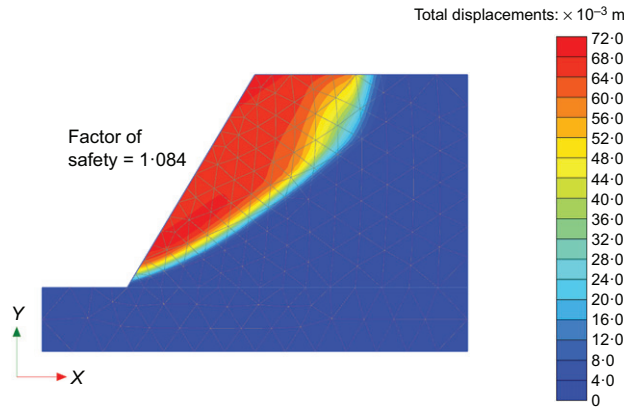

Fig. 11. Illustrative example: failure mechanism for homogeneous c–ϕ soil slope corresponding to $k_h = 0{\cdot}1$ and $k_v = 0{\cdot}05(\downarrow)$. A full-colour version of this figure can be found on the ICE Virtual Library (www.icevirtuallibrary.com)

Based on both use of the developed design chart and finite-element modelling, the illustrative example presented here clearly shows that, as k_h increases, the factor of safety of the slope decreases. Also, the factor of safety is found to be lower when k_v acts vertically upward compared to the downward case. Therefore, for the design of a soil slope during earthquakes, it is important to consider the effect of the vertical seismic coefficient with its proper direction along with the horizontal seismic coefficient.

CONCLUSIONS

In this paper, an attempt is made to explain how Taylor's chart for the homogeneous c–ϕ soil slope can be used during earthquakes considering the effect of both horizontal and vertical seismic loads. On the basis of the results and discussion presented in the previous section, the following general conclusions can be drawn.

(a) An analytical expression for the modified friction angle of the slope soil has been developed by incorporating the combined pseudo-static seismic coefficients k_h and k_v for use of Taylor's slope stability chart under generalised earthquake conditions.

(b) The value of friction reduction factor m is found to vary between 0 and 1 for a given slope angle and internal friction angle of the soil, irrespective of the value of k_h and k_v, as well as the direction of k_v.

(c) The greater the value of horizontal seismic coefficient with vertical seismic coefficient, the lower is the friction reduction factor m for a given angle of internal friction, which in turn gives rise to a higher stability number from Taylor's chart, resulting in a lower factor of safety. This implies that, under seismic loads, a soil slope is more unstable under the effect of vertical seismic load.

(d) The factor of safety of a slope with upward direction of k_v is more critical as compared to the k_v being in the downward direction or when k_v is not considered.

(e) For a higher slope inclination (e.g. $i = 75°$), an increase in horizontal seismic coefficient with vertical seismic coefficient being vertically upward, the friction reduction factor m for the slope may decrease significantly for modified friction angle, ϕ_m, to become zero. In this condition, soil may undergo undrained saturated loading condition, and hence it is recommended to consider the vertical seismic coefficient with its proper direction in order to have a safe design of the slope.

(f) The illustrative example solved based on both use of the developed design chart and the finite-element modelling may help practising engineers to design any specific homogeneous c–ϕ soil slope with simple profiles under generalised conditions of horizontal and vertical seismic loads using the analytical concepts and design charts presented in this paper with full confidence. It is important to note that the developed design charts as presented here are not applicable to seismic stability of slopes having non-standard profiles and consisting of non-homogeneous soil properties. In such cases, the numerical analysis will be of great help.

NOTATION

c	cohesion of the soil (kPa)
$c/F\gamma H$	stability number (dimensionless)
F	factor of safety (dimensionless)

F_h horizontal force due to earthquake (N/m)
F_v vertical force due to earthquake (N/m)
H height of the slope (m)
i angle of inclination of the slope with horizontal (degrees)
k_h horizontal seismic coefficient (dimensionless)
k_v vertical seismic coefficient (dimensionless)
l/d moment arm ratio (dimensionless)
m friction reduction factor (dimensionless)
P area component (m^2)
Q area component (m^2)
R radius of circular arc (m)
S total resisting force of the soil (N/m)
s shear strength of the soil (kPa)
W weight of the sliding mass (N/m)
α_0 angle with the horizontal chord of the slope (degrees)
β_0 central angle of the slope (degrees)
γ unit weight of the soil (N/m^3)
γ_E effective total unit weight of the soil (N/m^3)
σ total normal stress (kPa)
ϕ angle of initial friction (degrees)
ϕ_m modified friction angle due to generalised earthquake (degrees)

REFERENCES

Al-Defae, A. H., Caucis, K. & Knappett, J. A. (2013). Aftershocks and the whole-life seismic performance of granular slopes. *Géotechnique* **63**, No. 14, 1230–1244, https://doi.org/10.1680/geot.12.P.149.

Aoi, S., Kunugi, T. & Fujiwara, H. (2008). Trampoline effect in extreme ground motion. *Science* **322**, No. 5902, 727–730.

Arredi, F. (1966). A re-examination of the friction circle method for the stability analysis of slopes. *Meccanica* **1**, No. 3, 48–68.

Bardet, J. P., Oka, F., Sugito, M. & Yashima, A. (1995). *Preliminary investigation report of the great Hanshin earthquake disaster*. Los Angeles, CA, USA: Department of Civil Engineering, University of Southern California.

BIS (Bureau of Indian Standards) (2002). IS 1983: Indian standards criteria for earthquake resistant design of structures, part 1. New Delhi, India: BIS.

Bishop, A. W. (1955). The use of the slip circle in the stability analysis of slopes. *Géotechnique* **5**, No. 1, 7–17, https://doi.org/10.1680/geot.1955.5.1.7.

Cheng, Y. M. & Lau, C. K. (2014). *Slope stability analysis and stabilization: new methods and insight*. London, UK: Taylor & Francis.

Chopra, A. K. (1966). The importance of vertical component of earthquake motion. *Bull. Seismol. Soc. Am.* **56**, No. 5, 1163–1175.

Chowdhury, R., Flentje, P. & Bhattacharya, G. (2010). *Geotechnical slope analysis*. Boca Raton, FL, USA: CRC Press.

Das, B. M. (2010). *Principles of geotechnical engineering*, 7th edn. Stamford, CT, USA: Cenage Learning.

Duncan, J. M., Wright, S. G. & Brandon, L. T. (2014). *Soil strength and slope stability*. New York, NY, USA: Wiley.

Griffiths, D. V. & Lane, P. A. (1999). Slope stability analysis by finite elements. *Géotechnique* **49**, No. 3, 387–403, https://doi.org/10.1680/geot.1999.49.3.387.

Janbu, N. (1954). Application of composite slip surfaces for stability analysis. *Proceedings of European conference on stability of earth slopes*, Stockholm, Sweden, vol. 3, pp. 43–49.

Lew, M. (1991). Characteristics of vertical ground motions recorded during the Loma Prieta earthquake. *Proceedings of the 2nd international conference on recent advances in geotechnical engineering and soil dynamics*, St. Louis, MO, USA, pp. 1661–1666.

Ling, H. I. & Leshchinsky, D. (1998). Effects of vertical acceleration on seismic design of geosynthetic-reinforced soil structures. *Géotechnique* **48**, No. 3, 347–373, https://doi.org/10.1680/geot.1998.48.3.347.

Ling, H. I., Leshchinsky, D. & Mohri, Y. (1997). Soil slopes under combined horizontal and vertical seismic accelerations. *Earthquake Engng Structural Dynamics* **26**, No. 12, 1231–1241.

Ling, H. I., Mohri, Y. & Kawabata, T. (1999). Seismic stability of sliding wedge: extended Francais – Culmann's analysis. *Soil Dynamics Earthquake Engng* **18**, No. 5, 387–393.

Majumdar, D. K. (1971). Stability of soil slopes under horizontal earthquake force. *Géotechnique* **21**, No. 1, 84–88, https://doi.org/10.1680/geot.1971.21.1.84.

Matsui, T. & San, K. C. (1992). Finite element slope stability analysis by shear strength reduction technique. *Soils Found.* **32**, No. 1, 59–70.

Morgenstern, N. R. & Price, V. E. (1965). The analysis of the stability of general slip surfaces. *Géotechnique* **15**, No. 1, 79–93, https://doi.org/10.1680/geot.1965.15.1.79.

Plaxis (2016). *Essential for geotechnical professionals*. Delft, the Netherlands: Plaxis.

Sarma, S. K. (1973). Stability analysis of embankments and slopes. *Géotechnique* **23**, No. 3, 423–433, https://doi.org/10.1680/geot.1973.23.3.423.

Sarma, S. K. (1979). Stability analysis of embankments and slopes. *J. Geotech. Engng Div., ASCE* **105**, No. GT12, 1511–1524.

Shukha, R. & Baker, R. (2008). Design implications of the vertical pseudo-static coefficient in slope analysis. *Comput. Geotech.* **35**, No. 1, 86–96.

Shukla, S. K. (2015). *Core concepts of geotechnical engineering*. London, UK: ICE Publishing.

Spencer, E. (1967). A method of analysis of the stability of embankments assuming parallel inter-slice forces. *Géotechnique* **17**, No. 1, 11–26, https://doi.org/10.1680/geot.1967.17.1.11.

Stewart, J. P., Bray, J. D., Seed, R. B. & Sitar, N. (1994). *Preliminary report on the principal geotechnical aspects of the January 17, 1994 Northridge earthquake*, Report UCB/EERC-94/08. Berkeley, CA, USA: Earthquake Engineering Research Centre, University of California.

Taylor, D. W. (1937). Stability of earth slopes. *J. Boston Soc. Civ. Engrs* **24**, No. 3, 197–246.

Taylor, D. W. (1948). *Fundamentals of soil mechanics*. New York, NY, USA: Wiley.

Terzaghi, K., Peck, R. B. & Mesri, G. (1996). *Soil mechanics in engineering practice*. New York, NY, USA: Wiley.

USACE (US Army Corps of Engineers) (1989). *EM 1110-2-2502: Engineering and design of retaining and flood walls*. Washington, DC, USA: USACE.